applied sciences

MDPI

Review

Recent Advances in Femtosecond Laser-Induced Surface Structuring for Oil–Water Separation

Ali Sami Alnaser [1,2,*], Sharjeel Ahmed Khan [1,2,*], Rashid Ashirovich Ganeev [2] and Emmanuel Stratakis [3,4]

1 Department of Physics, American University of Sharjah, Sharjah 26666, UAE
2 Material Science and Engineering Research Institute (MSERI), American University of Sharjah, Sharjah 26666, UAE; rashid_ganeev@mail.ru
3 Institute of Electronic Structure and Laser, Foundation for Research and Technology-Hellas, 71110 Heraklion Crete, Greece; stratak@iesl.forth.gr
4 Department of Physics, University of Crete, 71003 Heraklion Crete, Greece
* Correspondence: aalnaser@aus.edu (A.S.A.); sakhan@aus.edu (S.A.K.)

Received: 19 March 2019; Accepted: 10 April 2019; Published: 15 April 2019

Abstract: Femtosecond (FS) laser-induced surface structuring is a robust, maskless, non-contact, and single-step process for producing micro- and nanoscale structures on a material's surface, which remarkably alters the optical, chemical, wetting, and tribological properties of that material. Wettability control, in particular, is of high significance in various applications, including self-cleaning, anti-fouling, anti-icing, anti-corrosion, and, recently, oil–water separation. Due to growing energy demands and rapid industrialization, oil spill accidents and organic industrial discharges frequently take place. This poses an imminent threat to the environment and has adverse effects on the economy and the ecosystem. Oil–water separation and oil waste management require mechanically robust, durable, low-cost, and highly efficient oil–water manipulation systems. To address this challenge superhydrophobic–superoleophilic and superhydrophilic–underwater superoleophobic membrane filters have shown promising results. However, the recyclability and durability issues of such filters are limiting factors in their industrial application, as well as in their use in oil spill accidents. In this article, we review and discuss the recent progress in the application of FS laser surface structuring in producing durable and robust oil–water separation membrane filters. The wide variety of surface structures produced by FS laser nano- and micromachining are initially presented here, while the excellent wetting characteristics shown by specific femtosecond-induced structures are demonstrated. Subsequently, the working principles of oil–water separation membranes are elaborated, and the most recent advances in the topic are analyzed and discussed.

Keywords: superhydrophobic; superoleophobic; femtosecond laser; superhydrophilic; oil–water separation

1. Introduction

Surface structuring using femtosecond (FS) pulses gives rise to spatially resolved micro/nanometer-sized features that are attributed to the reduced thermal and mechanical effects upon the ultrafast laser–material interaction [1,2]. It is a novel technique for precise control of a wide range of properties on virtually any type of material, including optical, mechanical, chemical, wetting, biological, and tribological properties [3]. As a result, FS laser-induced surface structures are used in a broad range of applications, including plasmonics, photonics, optoelectronics, photovoltaics, biomedicine, microfluidics, self-cleaning, and oil–water separation. For example, highly absorptive, black metallic [4], and semiconducting [5] surfaces formed by FS laser structuring are used in photovoltaics [6], as well

as in stealth technology [7], to entirely absorb ultraviolent -visible (UV–Vis) and infrared (IR) radiation. In addition, FS laser-fabricated, pigment-free, colored metals [8,9] and iridescent surfaces [10] can be applied for the fine-tuning of surface optical properties. Such colors are due to the plasmonic absorption at specific wavelengths featured by the laser-induced surface structures. Moreover, FS laser surface structuring can significantly alter the wetting properties of different materials. Inspired by the lotus leaf found in nature, superhydrophobic surfaces have been generated for applications in self-cleaning, anti-icing, drag reduction, corrosion resistance, and water harvesting [11–13]. In contrast to superhydrophobic surfaces, FS laser structuring can also provide, under certain irradiation conditions, surfaces capable of engulfing significant amounts of liquid, called super-wicking surfaces [14,15]. This effect is so strong that liquid could be transported uphill, against the gravitational pull, onto the structured surface. Recently, wettability control by varying the number of pulses and laser fluence in titanium [16] and copper [17], respectively, has been achieved by FS laser processing. It has been found that the number of incident pulses, pulse energy, laser fluence, and environment are important factors in realizing different levels of wettability [18,19]. Moreover, superhygrophobic surfaces recently fabricated by FS laser are able to repel complex liquid droplets, such as glucose, cola, juice, saline, and bovine serum albumin in water [20]. Other applications of FS laser-induced surface processing include the structuring of tissue engineering scaffolds showing enhanced cell adhesion properties [21–23], signal intensification for surface-enhanced Raman spectroscopy [24], enhancement of X-ray generation and photoelectron emission and manipulation of tribological properties [25,26].

The superior precision and accuracy of FS laser-induced surface structuring is a direct consequence of the shorter pulse duration and, thus, the laser–material interaction time [27]. In the case of longer pulses, the thermal energy generated upon melting diffuses around the irradiation spot, giving rise to the creation of heat-affected zones (HAZs). Above the material damage threshold, the HAZ has a detrimental effect on the integrity of the material by producing microcracks together with micropores. Besides this, when using longer pulses, the ablated material causes recast layers and surface debris, resulting in poor fabrication resolution. All such effects are avoided upon using FS laser pulses, due to the faster ablation process, i.e., rapid vaporization and material removal. Furthermore, FS laser surface structuring has various advantages compared with other techniques, such as photolithography, electron or ion beam; andmechanical and chemical methods. Such techniques involve multiple steps and tedious sample preparation and require vacuum conditions and hazardous chemicals. In conclusion, FS laser surface structuring is a simple, maskless, single-step, and non-contact process, enabling the controllable fabrication of various complex two-dimensional (2D) and three-dimensional (3D) structures [28–33] with high precision, as presented in Figure 1.

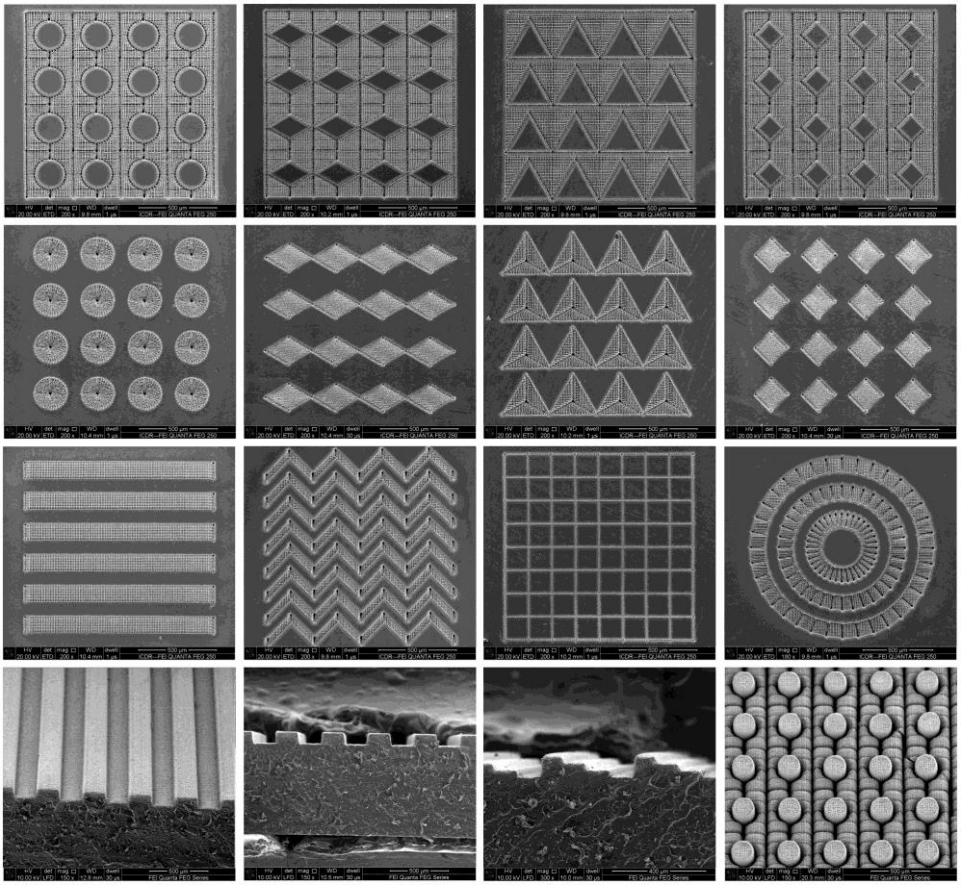

Figure 1. Various two-dimensional (2D) and three-dimensional (3D) structures formed by femtosecond (FS) laser surface structuring under various ablation conditions [32]. Reproduced with permission from [32] line 1–3 Copyrights Royal Society of Chemistry 2015. Line 4 copyrights Elsevier 2014.

The interaction of FS laser pulses with matter involves several processes and phenomena, taking place on short timescales. During the first moments of interaction, instantaneous excitation of electrons occurs due to linear or non-linear photon absorption processes. The former takes place in metallic materials—contrary to semiconducting and dielectric ones—where non-linear absorption processes become more pronounced. As a result of photon absorption, the electron temperature increases to much higher values compared with that of the lattice, because electron–electron interaction is much faster than electron–phonon coupling. Subsequently, the hot electrons and cold lattice reach equilibrium in a few picoseconds through electron diffusion and electron–phonon interaction [34]. This two-temperature model is widely used to interpret the laser–matter dynamics on the electronic level, prior to the establishment of thermal equilibrium. With regard to laser-induced surface structures, the electron–phonon interaction is a key factor in understanding their formation. In particular, the energy transfer from the electrons to the lattice depends on the electron–phonon coupling constant; the higher this constant, e.g., in metals, the faster the electron-to-lattice energy transfer occurs [34]. Furthermore, the energy accumulation on the material's surface and, therefore, the hydrodynamics of the molten pool leading to laser-induced self-assembled structures under non-ablation conditions [35] are highly dependent on the electron–phonon coupling constant.

Figure 2 shows the typical setup for FS laser-based surface structuring. The laser beam from the FS laser source is focused on the sample mounted on an XYZ translation stage controlled by a computer program. A combination of proper optics and lenses guides the laser beam to the sample. An electromechanical shutter placed in the beam's path interrupts the laser beam in raster scanning or spot-by-spot processing after a particular number of laser shots. The joulemeter is used to measure the energy deposited on the surface of the sample in real time. By controlling the laser fluence,

wavelength, repetition rate, number of pulses, and pulse duration, various surface structures are formed on different materials.

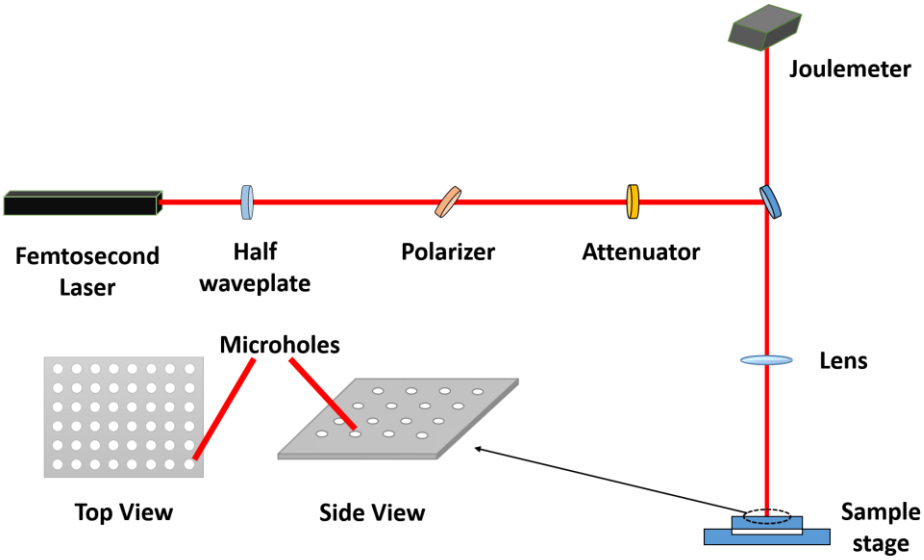

Figure 2. Typical setup used for femtosecond laser surface structuring and microfabrication.

Over the last decade, FS laser-induced surface structures have been successfully used to control the wetting response of materials [12], especially for the fabrication of surfaces exhibiting extreme wetting properties, from superhydrophobic to superhydrophilic and from superoleophobic to superoleophilic. Due to their remarkable superwetting characteristics, FS laser surface structures have recently been employed for applications in oil–water separation. In this article, we will critically review the extreme wetting properties reported for the FS laser-induced surface structures, as well as the research progress on the production of oil–water separation membranes by means of FS laser micro/nano fabrication.

2. Femtosecond Laser-Induced Self-Organized Periodic Surface Structures (LIPSS)

Apart from the complex, patterned surfaces attained by FS laser micromachining under ablation conditions, surface processing by FS lasers can also give rise to various submicron- and micron-sized, self-organized laser-induced periodic surface structures (LIPSS) created under practically non-ablative conditions [27,35]. Figure 3 represents an example of the different LIPSS structures attained on silicon upon irradiation with different numbers of FS pulses at a constant incident fluence. With a low number of pulses, the formation of laser-induced surface ripples perpendicular to the laser beam polarization occurs. Upon increasing the number of pulses, the formation of supra-wavelength laser-induced surface grooves (LISG), oriented parallel to the beam polarization, takes place. Further increasing the number of incident pulses gives rise to the creation of a quasi-periodic array of FS laser-induced surface micro-spikes (LISS) [2].

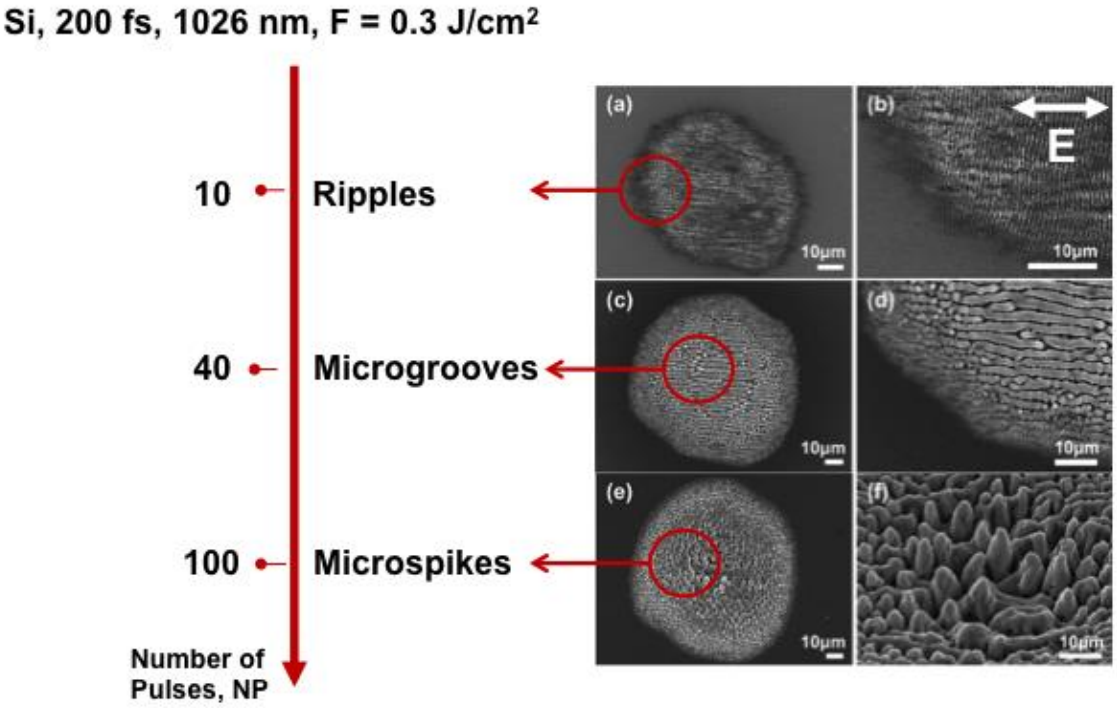

Figure 3. Different types of femtosecond (FS) laser-induced self-organized periodic surface structures (LIPSS) [2].

2.1. Laser-Induced Surface Ripples

Laser-induced surface ripples (LISR) are formed on solid surfaces when the polarized laser beam interacts with a material, generating a periodic spatial distribution of the electromagnetic field and, in turn, a periodic spatial distribution of the melt profile at micrometer and sub-micrometer scales. LISR are widely studied, and a broad variety of such structures can be created due to their dependence on laser fluence, number of pulses, angle of laser beam incidence, wavelength, and polarization direction. The LISR formation mechanism and its dependence on various parameters have already been reviewed in [36]. Although LISR have been generated by long laser pulses [37], the advancement of FS lasers has revealed exciting ways to create such structures with improved spatial resolution. LISR have found applications in creating different structural colors [9,38] and anti-reflecting coatings [4,7] and in controlling surface wetting properties [39].

Given that the LISR formation and orientation are directly related to the laser polarization state [40,41], control over the beam polarization is a unique tool to fabricate complex LISR morphologies comprising more than a single spatial frequency, as shown by LISR fabricated with linearly polarized light [30,40]. Such frequencies can be efficiently tuned upon variation of the central laser wavelength and the number of pulses per irradiation area [36]. Figure 4 presents examples of complex LISR structures fabricated upon laser processing with three different polarization states on Ni [30] surfaces. Considering that wetting properties are highly dependent on the shape, size, and orientation of the surface structures, the polarization control of LISR should be a useful tool to realize an ensemble of complex morphologies, facilitating the elegant tuning of the wettability of materials used for oil–water separation.

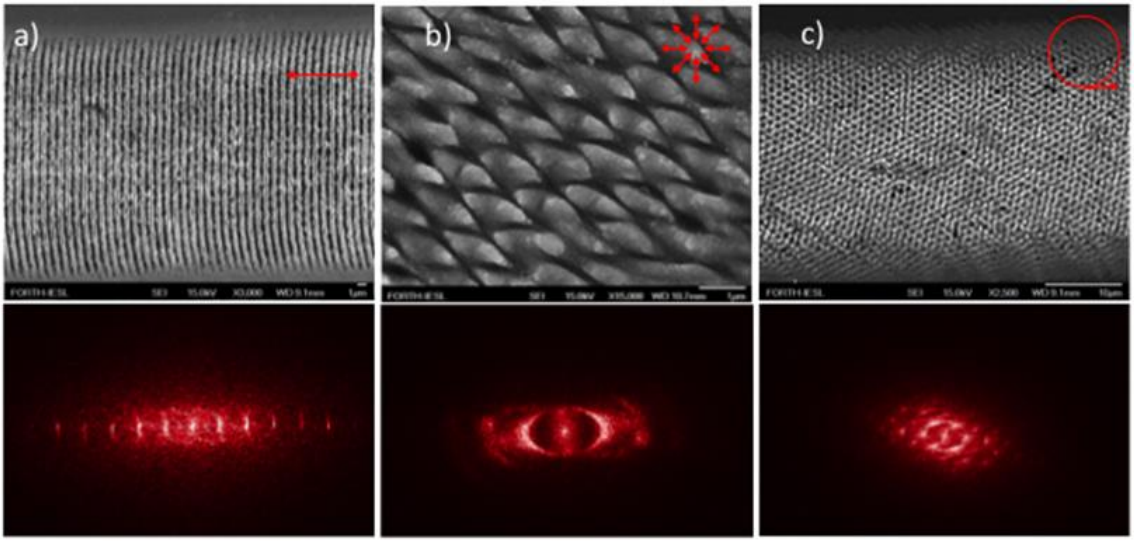

Figure 4. Various LIPSS types formed by FS laser pulses of different polarization: (**a**) Grating-like Laser-induced surface ripples (LISR) formation fabricated with linear polarization; (**b**) rhomboidal multi-directional surface structures produced by radial polarization; and (**c**) columnar structures fabricated by circular polarization. The corresponding fast Fourier transform (FFT) diagrams are also shown, revealing the different spatial frequencies included in each structure [30].

2.2. Microgrooves

Although LISR formation occurs for low excited electron densities, laser-induced surface grooves (LISG) appear for large ones. The increased temperature due to the relaxation process leads to a thermal gradient and the formation of convection rolls in the molten material because of the Marangoni effect, which eventually leads to sub-wavelength microgrooves [35]. As confirmed by both experimental studies and simulations, the LISG periodicity is an increasing function of the number of pulses [35]. LISG show higher superhydrophobicity compared with LISR and, therefore, are expected to be good candidates for oil–water separation [42].

2.3. Conical Spikes or Columnar Structures

Conical or columnar structures can also be formed by laser surface structuring at optimized fluence, ablation threshold, number of pulses, scanning speed, and type of material [43]. For example, Figure 5a–d shows columnar structures covered with nanostructures on a titanium surface with a TiSa Laser (65 FS, $\lambda = 800$ nm, 1 kHz, 0.35 J/cm^2) at different numbers of pulses. It was observed that columnar structures began to form when the laser exposure reached 100 shots, while they became more prominent upon increasing the number of pulses [21]. This finding indicates that the geometrical features of columnar structures can be manipulated by optimizing the number of incident pulses. Moreover, the pulse energy and the type of material are additional factors that need to be considered. Indeed, the higher damage threshold for hard materials (e.g., for titanium it should be above 0.5 J/cm^2 [44]) and the lower one for soft materials (e.g., for aluminum it should be below 0.16 J/cm^2 [44]) need to be taken into account upon optimizing the columnar structures. Furthermore, the irradiation environment may influence the formation of conical structures. For instance, conical structures grown on titanium [45] and silicon [2] are taller and sharper when irradiated in the presence of SF_6 gas. Figure 5e,f shows an Si surface irradiated in air and a SF_6 gas environment with an average of 500 laser pulses (180 FS, $\lambda = 800$ nm, F = 2.47 J/cm^2). The conical structures show remarkable superhydrophobicity compared with LISR and LISG [42]. Therefore, such structures are expected to be promising candidates for oil–water separation.

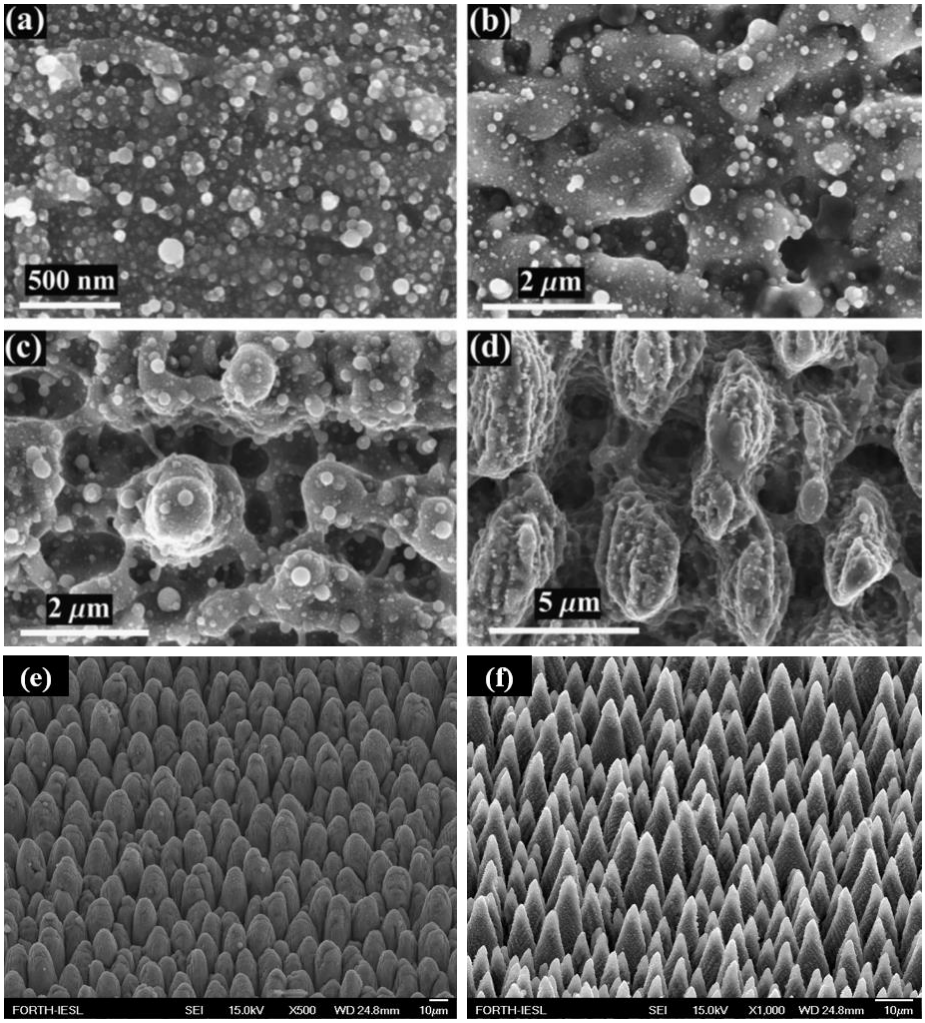

Figure 5. (**a**–**d**) Titanium sample irradiated with F = 0.35 J/cm^2 (**a**) 1 laser shot, (**b**) 40 laser shots, (**c**) 100 laser shots, and (**d**) 200 laser shots [21]. Reproduced with permission from [21] Elsevier 2007. (**e**,**f**) Black silicon surfaces obtained upon FS laser processing in air and SF_6 ambient conditions, respectively [2].

3. Wettability Control

The wetting properties of materials have great significance in a wide range of applications and are thus critical for understanding the mechanism of oil–water separation. The wettability of a material comes as the result of the synergy of the surface morphology and chemistry [46]. Inspired by the remarkable superhydrophobic properties of the natural lotus leaf, researchers have mimicked the leaf morphology and surface chemistry to produce artificial surfaces showing extreme water repellency [47]; water droplets do not wet and bounce as a perfect elastic sphere on such surfaces and easily roll off, giving rise to a self-cleaning effect. Lotus leaf microscopic analysis has revealed the presence of hierarchical surface structures, comprising microconical asperities decorated with a layer of waxy nanohairs. Such hierarchical microstructures are behind the self-cleaning features of the lotus leaf, which keep it lush, green, and clean [47]. As a consequence of such remarkable properties, artificially prepared superhydrophobic surfaces have found a wide range of applications in self-cleaning, anti-icing, anti-corrosion, drag reduction, and oil–water separation uses [48,49]. Superhydrophobic surfaces exhibit a water contact angle (WCA) higher than 150° and a roll-off angle (sliding angle (SA) in Figure 6b) lower than 10°. Based on the same principles, superoleophobic surfaces exhibit an oil contact angle (OCA) higher than 150° and a roll-off angle lower than 10°. On the other hand, superhydrophilic and superoleophilic surfaces show contact angles of ~0° for water and oil, respectively.

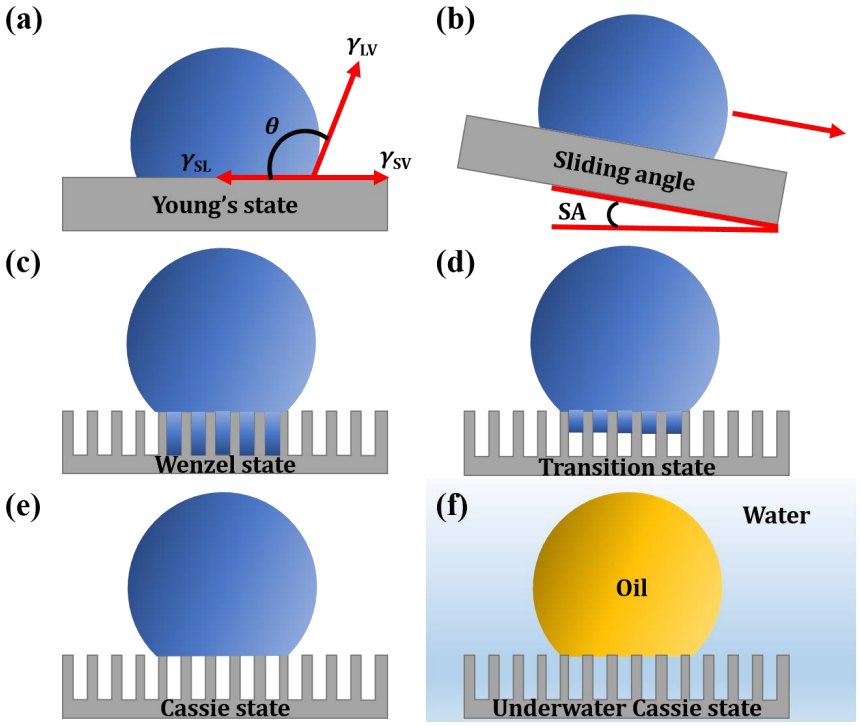

Figure 6. Different wetting states of water and oil droplets. (**a**) Young state of a droplet on a flat surface; (**b**) definition of the sliding angle (SA) or roll-off angle; (**c**) Wenzel state where the liquid completely wets the surface structures; (**d**) transitional or partial wetting state; (**e**) Cassie–Baxter state, where the droplet sits on the microstructures and air is trapped beneath it; and (**f**) oil droplet underwater in the Cassie–Baxter state.

4. Oil–Water Separation Mechanism

The superwetting characteristic of water and oil phases on a solid surface is predominantly responsible for oil–water separation in membrane technology. The wetting response of a surface to a liquid is characterized by the contact angle of a liquid droplet on the surface. When such a droplet is placed on a surface, it forms a hemispherical shape due to the minimization of the surface free energy. The contact angle, θ, depending on the surface free energy of the solid, liquid, and vapor interfaces, is described by Young's equation [50]:

$$\cos\theta = (\gamma_{SV} - \gamma_{SL})/\gamma_{LV} \quad (1)$$

where γ_{SV}, γ_{SL}, and γ_{LV} are the surface free energy of the solid/vapor, solid/liquid, and liquid/vapor interfaces, respectively (Figure 6a).

Young's state explains the wettability response of the material on an ideally flat surface. However, microscopic surface roughness has a crucial influence on the wetting response. The effect of the surface roughness on the wettability has been widely described by two different models (Figure 6c,d). In the Wenzel model, the liquid is assumed to completely penetrate the entire rough surface, described as a homogeneous wetting state, without leaving any air pockets underneath. The apparent contact angle, θ_w, is then given by a modified Young's equation:

$$\cos\theta_w = r(\gamma_{SV} - \gamma_{SL})/\gamma_{LV} = r\cos\theta \quad (2)$$

where the roughness factor "r" is the ratio of the unfolded to the projected surface area [51] and θ is the contact angle on a flat surface of the same nature as the rough. Because r is always greater than unity, this model predicts that the contact angle will decrease/increase with surface roughness for an initially hydrophilic ($\theta < 90°$)/hydrophobic ($\theta > 90°$) surface. In other words, a hydrophobic rough surface

becomes more hydrophobic, while a hydrophilic one becomes more hydrophilic. Furthermore, contrary to the Wenzel's droplet state, Young's state, i.e., an ideally flat surface, exhibits limited hydrophobicity, as the effect of the surface energy alone is not enough to realize superhydrophobicity.

Contrary to the Wenzel state, in the case of the Cassie–Baxter droplet state (Figure 6d), the droplet sits on the surface microstructures, and air pockets are trapped beneath the liquid [52]. In this case, the apparent contact angle θ_{CB} is provided by the following relation:

$$\cos\theta_{CB} = f\cos\theta + f - 1 \quad (3)$$

where f is the area fraction of the liquid in direct contact with the surface structures and θ is the Young's contact angle. As f is always lower than unity, this model always predicts the enhancement of hydrophobicity independently of the value of the initial contact angle θ. In practice, a transitional stage between the Wenzel and Cassie state is more likely to occur, in which the liquid only partially permeates the rough surface (Figure 6e). As a result, the droplet forms a composite solid–liquid/air–liquid interface with the surface in contact. In this case, the apparent contact angle, θ_{tr}, is an average of the flat surface, θ, and the value for suspending over the flat surface (that is, 180°) is given by [53]:

$$\cos\theta_{tr} = r_f f'\cos\theta + f' - 1 \quad (4)$$

where f' defines the fraction of the projected solid surface that is wetted by the liquid and r_f is the roughness ratio of the wet area. When $f' = 1$ and $r_f = r$, Equation (4) turns into the Wenzel equation. In the extreme case of a superhydrophilic–underwater superoleophobic surface (Figure 6f), the droplet volume is adsorbed by the surface structures in air, but when an oil droplet is placed on the surface while it is immersed in water, it exhibits a high contact angle for oil. This is explained by extending the Cassie–Baxter or transition states for the oil droplet. To realize oil–water separation, two different approaches are commonly used, namely superhydrophobic–superoleophilic membranes or superhydrophilic–underwater superoleophobic membranes. In superhydrophobic–superoleophilic membranes, oil is adsorbed while the water is obstructed due to the non-wetting properties. However, a superhydrophilic–underwater superoleophobic membrane repels oil under water. The wetting response of the latter surface depends on the medium; thus, it is superhydrophilic and oleophilic in air, but when it is immersed in water, it becomes superoleophobic. As a consequence of this response, water passes through the membrane, whereas oil is obstructed, resulting in oil–water separation.

5. Oil–Water Separation via FS Laser Structuring

Oil–water separation was realized for the first time via a superhydrophobic and superoleophilic mesh. In particular, a rough microstructured polytetrafluoroethylene (PTFE) coating deposited on stainless mesh was used for separation [54]. It was reported that when an oil–water mixture is poured on the mesh, oil gets absorbed, while water is repelled due to the superhydrophobic–superoleophilic behavior of the prepared mesh. Over the past decade, superhydophobic–superoleophilic and superhydrophilic–underwater superoleophobic membranes have been produced using different techniques on various materials. Such techniques include electrochemical deposition, sol–gel process, chemical etching, lithography, spray and dip coating; and they have been employed to modify materials such as filter paper [55], cotton [56,57], fabric [58], wood [59], metallic meshes [60], and sponges/foams [55,61] for oil–water separation [62,63]. Moreover, oil–water separation has been reported for superhydrophilic–underwater superoleophobic surfaces [64]. Although such techniques have provided promising separation efficiencies, it was impossible to retain their special wetting characteristics for a prolonged time. This can be attributed to the corrosive action of the liquids, high temperature, friction, and mechanical wear and tear [65]. Moreover, most of the produced coatings were fragile and easily worn off by slight mechanical abrasion; as a result, the super-wetting properties significantly degraded over time.

Table 1. Oil–water separation filters/meshes realized by FS laser fabrication.

Material	Laser Structures	Fabrication Parameters	Chemical Treatment	Wettability Characteristic	Oil Separated	Ref.
FS Laser-Structured Meshes						
Janus mesh (side 1)	LISR	580 mW, 7.39 × 10^6 mJ/cm^2	1H,1H,2H,2H-perfluorodecyltriethoxysilane	Superhydrophobic–superoleophilic	Bean oil, n-heptane, methyl benzene	[66]
Janus mesh (side 2)	-	-	Graphene oxide	superhydrophilic–underwater superoleophobic	Perchloromethane, trichloromethane.	
Stainless steel	LISR	λ = 1030 nm, 250 FS, 75 kHz	-	superhydrophilic–underwater superoleophobic	Edible oil, diesel, crude oil, hexadecane, 1,2-dichloroethane.	[67]
FS Laser-Fabricated Arrays of Micro-Through Holes						
PTFE	-	λ = 800 nm, 50 FS, 1 kHz,	-	superhydrophobic–superoleophilic	petroleum ether, acid/base (HCl and KOH) solution,	[68]
Titanium	-	λ = 800 nm, 50 FS, 1 kHz, 3.1–15.5 J/cm^2	-	Superhydrophilic underwater–superoleophobic	petroleum ether, heptane, hexane, gasoline, crude oil, soybean, silicon oil	[69]
Aluminum	-	λ = 800 nm,104 FS, 1 kHz, 4–5 pulses/hole	1H,1H,2H,2H-perfluorodecyltriethoxysilane (PFDTES)	superhydrophilic underwater–superoleophobic superhydrophobic–superoleophilic	Octane, 1,2-dichloroethane	[70]

LISR: laser-induced surface ripples, PTFE: polytetrafluoroethylene.

On the contrary, FS laser microfabrication has shown exceptional results with respect to the realization of durable and reliable superwetting materials for efficient oil–water separation [62]. Table 1 summarizes the most important recent reports on this topic. In particular, oil–water separation filters have been formed by either FS laser drilling of micro-through holes in a thin sheet or growing hierarchical microstructures on a mesh surface via FS laser ablation. Oil–water separation has been realized with or without subsequent chemical functionalization [11,69,71]. Recently, FS laser surface structuring has been used to produce six different types of wettability for polydimethylsiloxane (PDMS) and aluminum surfaces [72,73]. FS laser-irradiated aluminum surfaces exhibit superhydrophilic, underwater superoloephobic, and underwater superaerophilic wettability characteristics. When the FS laser-structured aluminum surface is functionalized with 1H,1H,2H,2H-perfluorodecyltriethoxysilane, its wettability behavior changes completely to superhydrophobic, underwater superoleophilic, and underwater superaerophilic [72]. In the case of a FS laser-structured PDMS surface, superhydrophobic, underwater superoleophilic, and underwater superaerophilic wetting properties were observed. Further irradiation with oxygen plasma activated the PDMS surface by inducing Si-OH groups. As a result of oxygen plasma treatment, the PDMS wettability was switched from hydrophobic to hydrophilic. Therefore, superhydrophilic, underwater superoleophobic, and underwater superaerophobic wettability were realized [73]. In light of the above results, it can be concluded that wettability control via FS laser structuring is a promising tool for oil–water separation.

5.1. FS Laser-Structured Meshes

Liu et al. reported on a Janus wire mesh for oil–water separation (Figure 7) that exhibited different wettability on its opposite sides [66]. One side was superhydrophobic–superoleophilic, while the other side was superhydrophilic–underwater superoleophobic. Initially, LISR were formed on both sides of the copper mesh, and then, the superhydrophobic side was prepared by surface functionalization with 1H,1H,2H,2H-perfluorodecyltriethoxysilane. Similarly, the underwater superoleophobic side was formed via dipping into a graphene oxide aqueous solution. Figure 7a–h shows SEM images and the elemental map of both sides of the mesh, which confirm the modification with fluorosilane and graphene oxide, respectively. It was observed that the opposite wetting responses present on the same mesh facilitate the separation of light and heavy oils from water. For light oil separation, the superhydrophobic–superoleophilic side was brought in contact with the oil–water mixture, whereas for heavy oil separation, the oil–water mixture was placed on the superhydrophilic–underwater superoleophobic side. As a result, for both heavy and light oil–water mixtures, a separation efficiency greater than 99% was achieved.

Yin et al. used a FS laser to generate LISR on stainless-steel mesh for oil–water separation purposes [67]. Figure 8a,b shows an optical image of the mesh before and after laser treatment, respectively; following the laser treatment, the mesh color turned to black. Figure 8c–e shows that the uniform nanoripples, exhibiting a 500–800 nm period and an average depth of 130 nm, are covered with nanoparticles of variable sizes, formed upon FS laser treatment. Figure 8f,g presents the chemical composition of the pristine and laser-treated meshes. The latter showed an increase in oxygen content, attributed to the oxidation of Cr, Mn, and Fe present in the stainless steel. As a consequence of the laser treatment, the mesh wettability changed from having weak hydrophobicity in its pristine state to being superhydrophilic. Moreover, the underwater contact angle of a 1,2-dichloroethane oil droplet on the laser-processed mesh was equal to 157.2°, and the sliding angle was 5°. An oil–water separation process using laser-structured mesh is demonstrated in Figure 9a–d. An oil–water mixture was poured onto the pre-wetted laser-treated mesh positioned above two beakers at a ~25° tilt angle. It was observed that water passed through the mesh and dripped off into the first beaker, while oil was repelled and rolled off the mesh surface and was collected in a separate container. Laser-treated stainless-steel mesh was tested with different oil–water mixtures, and all showed high OCAs >150°, irrespective of oil type, and a high separation efficiency of 99%. The laser-processed mesh was quite

durable and chemically inert, considering that it retained its wetting characteristics even when it was rubbed repeatedly with sand paper and after being treated with 1 M HCl, 1 M NaOH, and 10% NaCl solutions. Such severe treatments validate the use of laser-structured mesh in harsh environments.

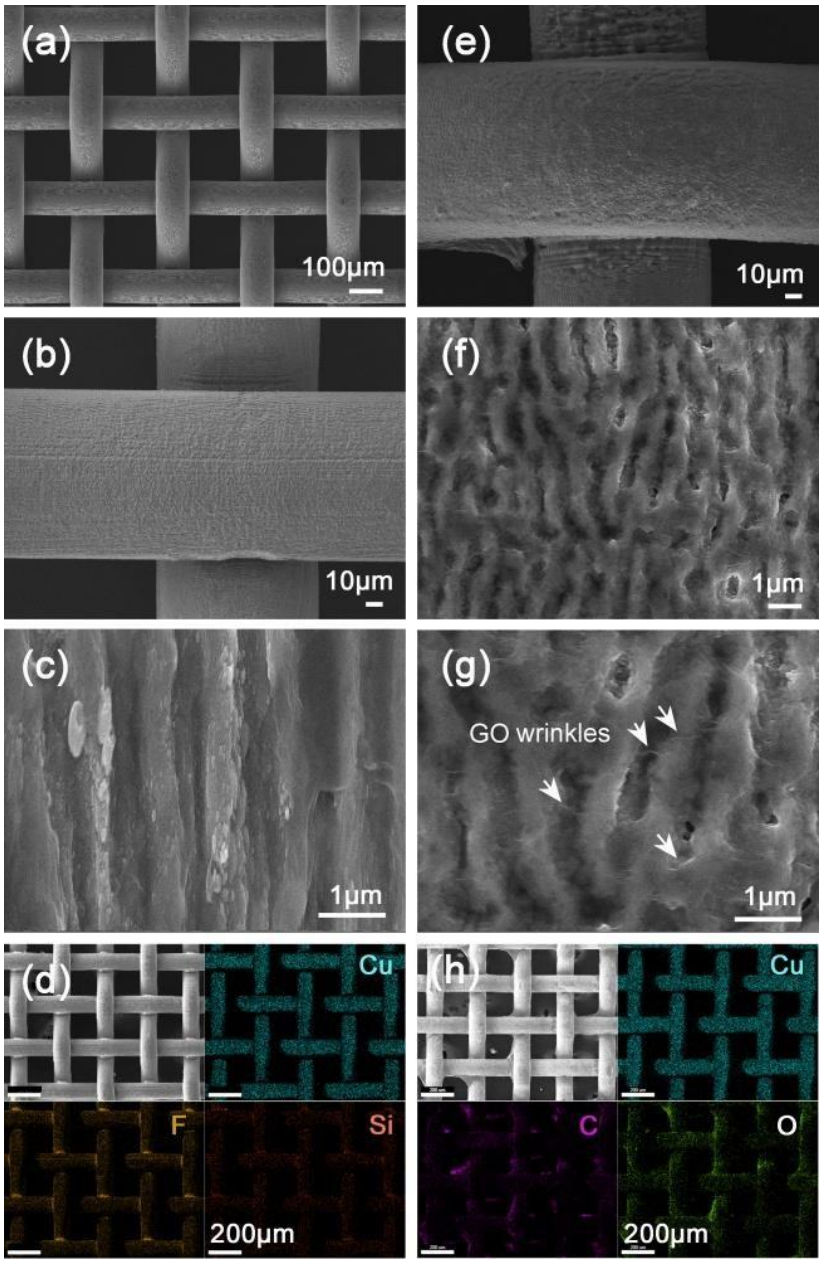

Figure 7. (**a**,**b**) SEM image of FS laser-structured Janus wire mesh. (**c**) Laser-structured fluorosilane-modified mesh (580 mW, 7.39 × 106 mJ/cm^2) at different magnifications. LISR with a period of 900 nm at fluorosilane-modified mesh. (**d**) Elemental map of fluorosilane-modified mesh showing the presence of fluorine and silicon. (**e**,**f**) Laser-structured GO-modified mesh (100 mW, 12.74 × 105 mJ/cm^2) at different magnifications. (**g**) LISR covered with GO wrinkles. (**h**) Elemental map of GO-modified mesh showing the high presence of oxygen and carbon [66]. Reproduced with permission from [66] Royal Society of Chemistry 2017.

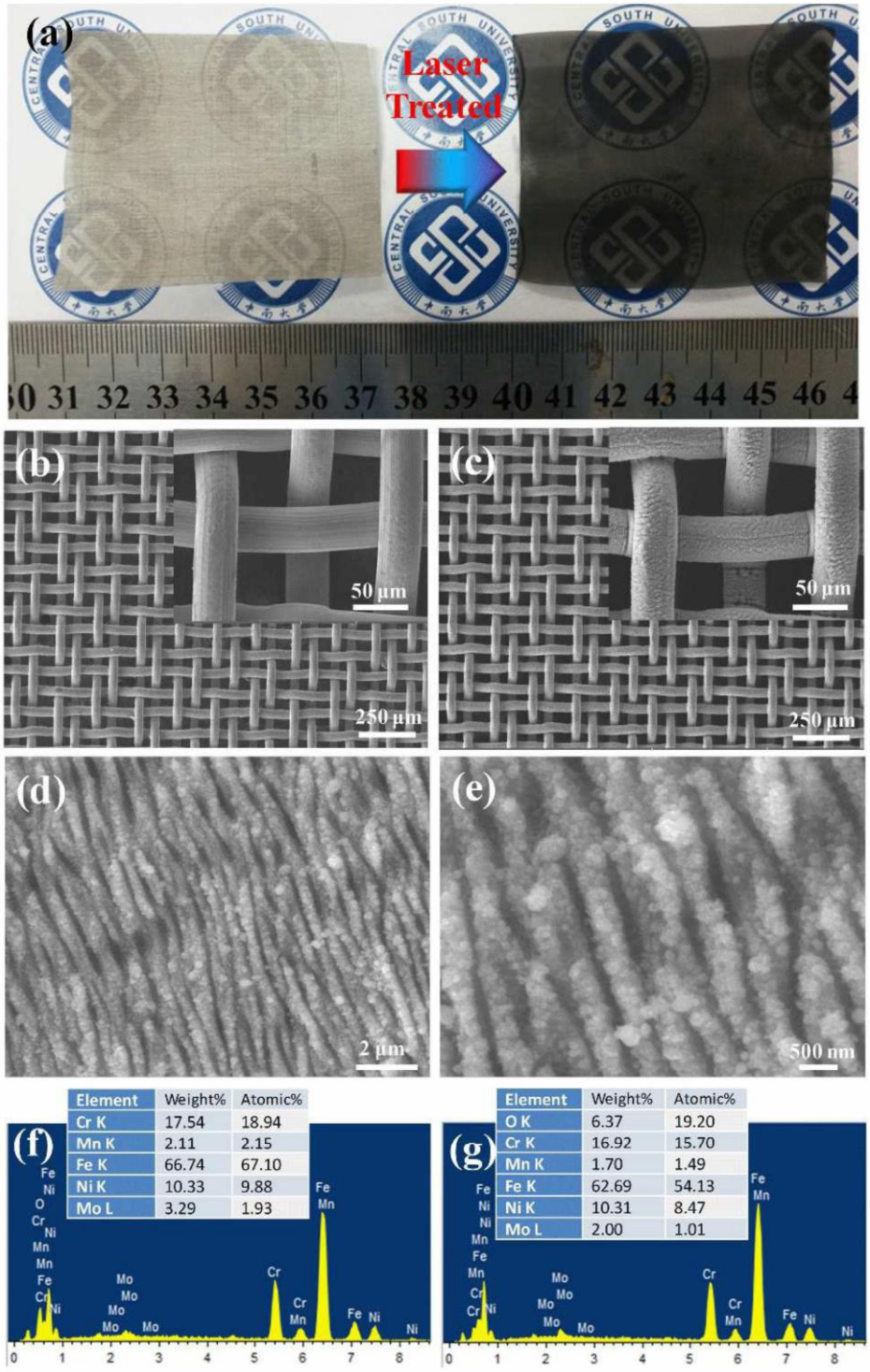

Figure 8. (**a**) Optical and (**b**,**c**) SEM images of stainless-steel mesh before and after FS laser treatment. (**d**,**e**) SEM images of LISR present on the FS laser-irradiated mesh, at different magnifications; (**f**,**g**) chemical composition analysis of the pristine and the laser-treated stainless-steel mesh [67]. Reproduced with permission from [67] Royal Society of Chemistry 2017.

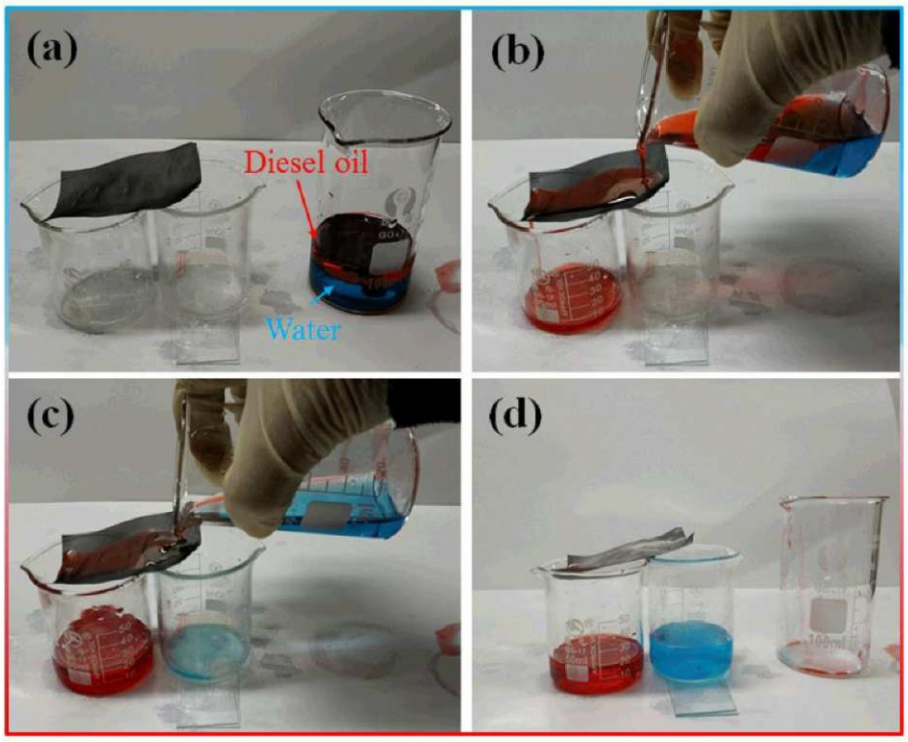

Figure 9. Oil–water separation with a superhydrophilic–underwater superoleophobic FS laser-treated mesh. Contrary to water, oil is repelled, while both the liquids are collected in separate containers [67]. Reproduced with permission from [67] Royal Society of Chemistry.

5.2. FS Laser Fabrication of Arrays of Micro-Through Holes

FS laser microfabrication was used to create rough microstructures on the surface of PTFE sheets, as shown in Figure 10a–c [68]. Following the laser ablation process, the PTFE sheet surface showed a porous structure, comprising highly dense protrusions with heights ranging from 300 nm to 2 μm. As a consequence, the laser-structured sheets showed both superhydrophobicity and superoleophilicity with static water and oil contact angles of 155.5° and nearly 0°, respectively (Figure 10d,e). Here, the surface structure enhanced the intrinsic hydrophobic characteristic of PTFE and rendered it superhydrophobic. Subsequently, an array of micro-through holes was formed by mechanical drilling from the backside of the ablated PTFE sheet. As a result, the drilled sheet displayed high efficiency with respect to oil–water separation. Additionally, it was also effective for the separation of strong acid/alkali substances from oil, indicating the high durability and chemical inertness of PTFE sheets in corrosive environments.

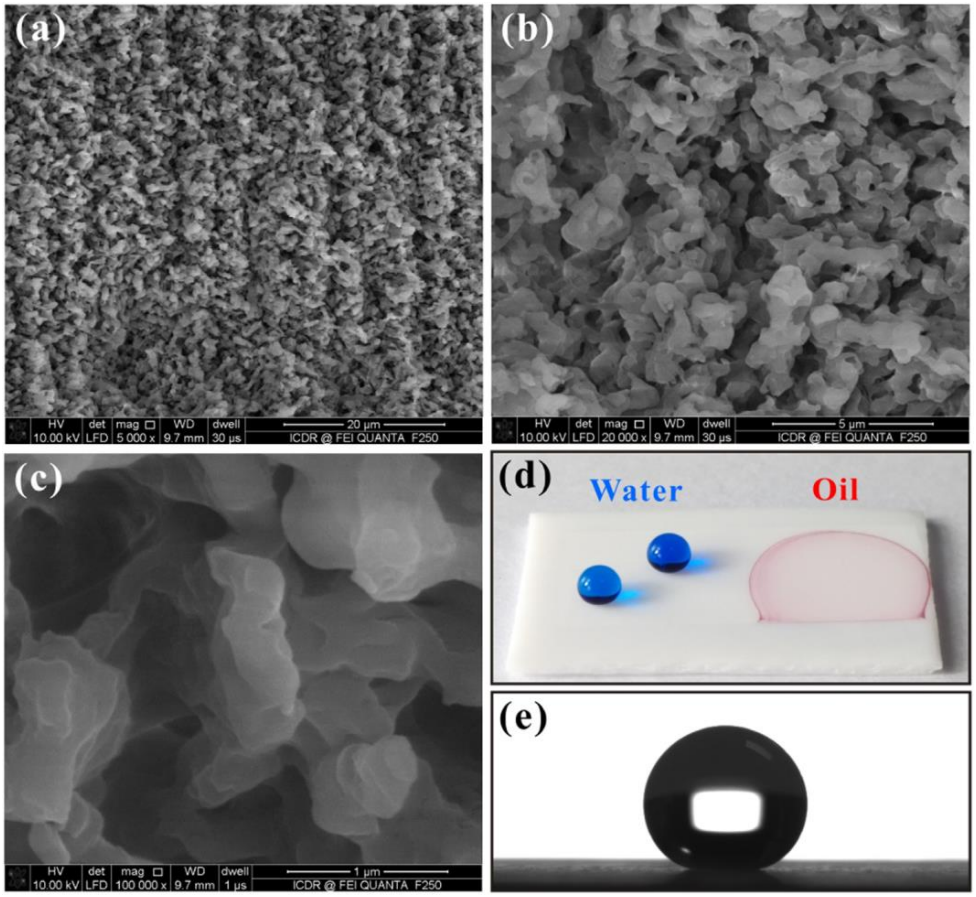

Figure 10. (**a**–**c**) SEM of FS laser surface structures on the PTFE surface at different magnifications. (**d**) Image of a water droplet and oil droplet on the PTFE structured surface. (**e**) Water contact angle measurement of the PTFE laser-structured surface [68]. Reproduced with permission from Elsevier 2016.

Li et al. employed a FS laser with 104 FS pulse duration and a 1 kHz repetition rate to drill an array of micropores on aluminum foil of 2.4–32 μm diameter and a period of 20–80 μm [70]. Figure 11a,b presents a typical SEM image of the drilled foil, showing that the micropores' sidewalls are decorated with nanostructures. Although the flat aluminum foil surface is inherently hydrophilic with a water contact angle of 53.9°, the laser-drilled foil became superhydrophilic, showing a water contact angle of 7.8°. As also shown in Figure 11c,d, the oil contact angle of octane and 1,2-dichloroethane was 153.5° and 153.1°, respectively. For the evaluation of the oil–water separation efficiency, oil–water mixtures were poured into a tube that contained a horizontally placed, laser-processed aluminum foil (Figure 12a–c). During the pouring process, water passed through the micropores, while the oil was inhibited due to the superoleophobic property of the foil. For the separation of heavy oil, a tube with a side opening was used, while the irradiated aluminum foil was placed vertically, as shown in Figure 12d–e. The separation process was completed within 31 s. The continuous separation of oil–water mixtures was additionally demonstrated (Figure 13). In that case, the laser-irradiated aluminum foil was modified with 1H,1H,2H,2H-perfluorodecyltriethoxysilane (Figure 13a). Owing to such functionalization treatment, the foil wetting properties changed from superhydrophilic–underwater superoleophobic to superhydrophobic–superoleophilic. Figure 13b shows a schematic representation of the continuous separation process. Both of the membranes (i.e., the laser-irradiated and functionalized one) were placed inside a tube with a side opening. It was observed that the water-selective membrane permitted water to pass through, whereas the oil-selective membrane permitted oil to pass through. The whole process was completed within 28 s. As a result, separation can be achieved by using just the gravity effect, with an efficiency of 99% for both light and heavy oil.

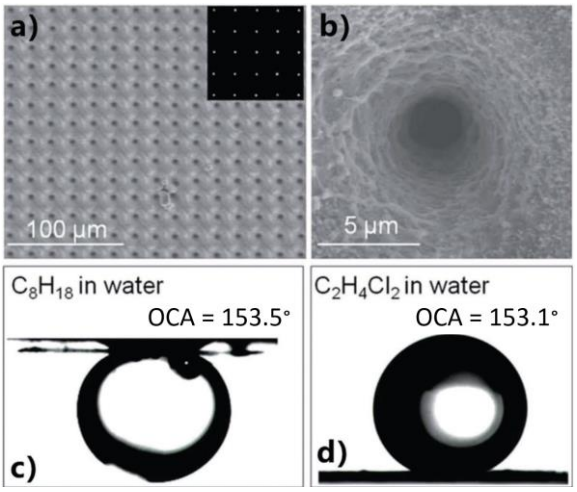

Figure 11. (**a**) SEM image of the micropores drilled in ultrathin aluminum foil by FS laser ablation; the inset shows that light can pass through the micropores' array. (**b**) Magnified image of the treated foil showing that the rim of the pores is decorated with microstructures; (**c**) underwater contact angle of a light oil (C_8H_{18}) droplet on the laser-treated aluminum foil; and (**d**) underwater contact angle of a heavy oil ($C_2H_4C_{l2}$) droplet on the laser-treated aluminum foil [70]. OCA: oil contact angle. Reproduced with permission from [70] Royal Society of Chemistry 2016.

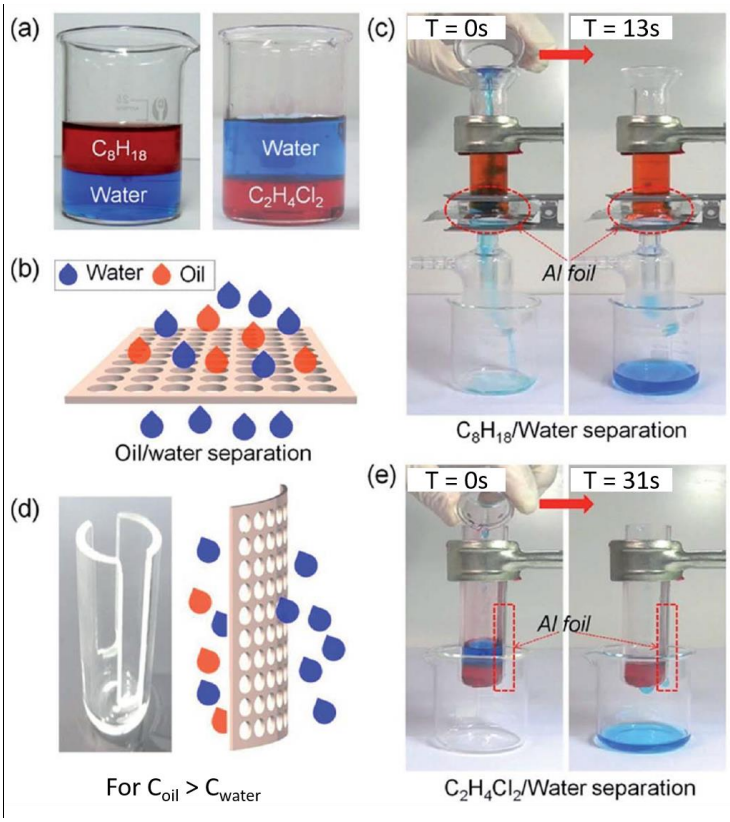

Figure 12. (**a**) Oil–water mixture of heavy and light oil. (**b**) Schematic of the light oil–water separation process; (**c**) oil–water separation was completed within 13 s in the case of the octane light oil. (**d**) Tube with side opening and schematic of the heavy oil–water separation process; (**e**) the heavy oil–water separation process was completed within 31 s [70]. Reproduced with permission from [70] Royal Society of Chemistry 2016.

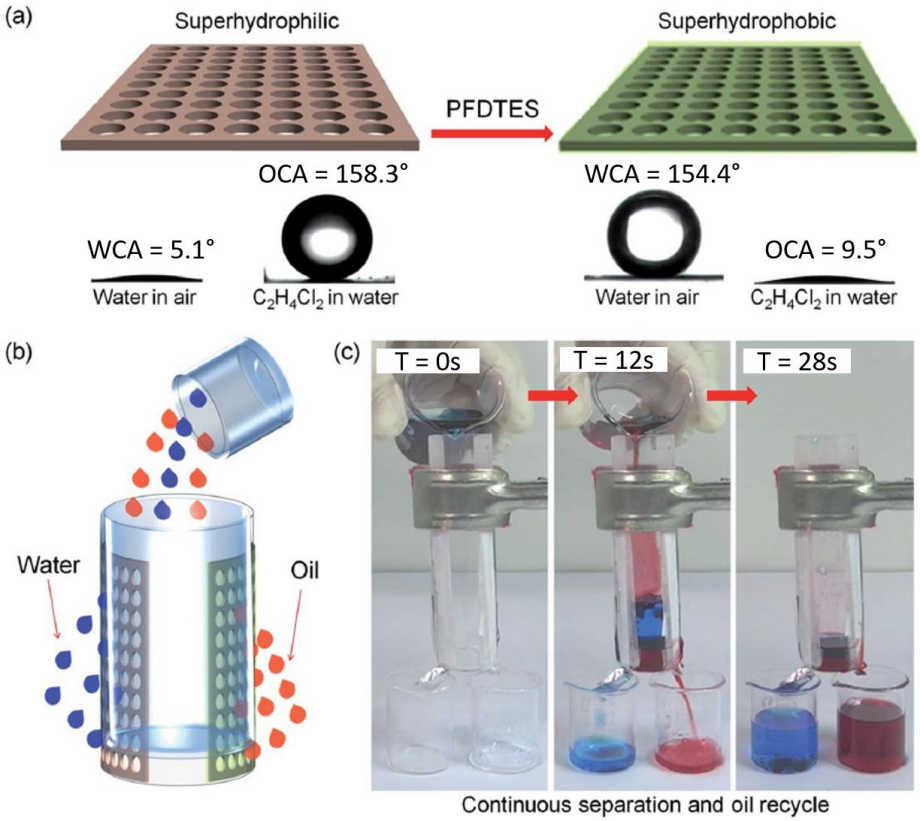

Figure 13. (**a**) Schematic of the modification of a FS laser-drilled aluminum foil with 1H,1H,2H,2H-perfluorodecyltriethoxysilane. Following this process, the water contact angle (WCA) turned from superhydrophilic (WCA ~5.1°) to superhydrophobic (WCA ~154.4°); (**b**) schematic illustration of the continuous separation of an oil–water mixture by superhydrophobic and superhydrophilic foil; (**c**) the continuous separation of an oil–water mixture, which was completed in 28 s [70]. WCA: water contact angle. Reproduced with permission from [70] Royal Society of Chemistry 2016.

In another approach, a FS laser-processed titanium membrane filter showed high oil–water separation efficiency [69]. In that case, the microholes formed with a spacing of 100–300 μm, using a laser fluence of 3.1–15.5 J/cm^2. In particular, the titanium filter prepared with a fluence of 12.4 J/cm^2 and 100 μm interspacing showed a remarkable separation efficiency of 99%, with high recyclability. Figure 14 shows a typical SEM image of the titanium membrane filter and the respective energy dispersive x-ray (EDX) analysis of the microholes. Laser ablation leads to the creation of microprotrusions and extensive oxidation of titanium due to oxygen presence in the ambient air.

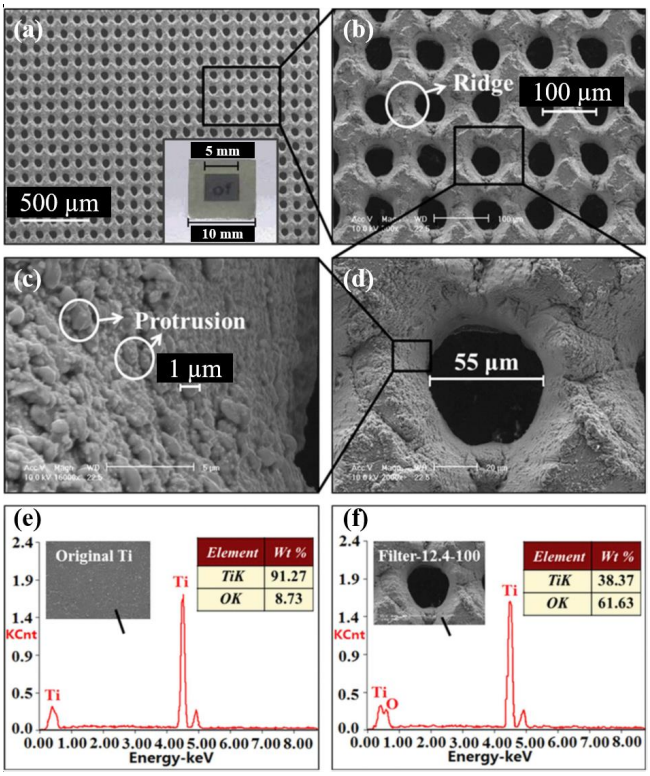

Figure 14. (**a**–**d**) SEM image of a FS laser-fabricated titanium membrane filter showing the presence of microprotrusions at the periphery of the microholes; (**e**,**f**) EDX analysis of the pristine and FS laser-treated titanium foil [69].

6. Summary and Outlook

In summary, FS laser surface structuring is a new technology that can be used to create micro- and nanostructures on virtually any type of material. As a consequence of its remarkable ability to control the morphological features at multiple length scales, FS laser processing is a unique tool to tune the wettability of solid surfaces. This capability demonstrates the great potential of FS structuring techniques for oil–water separation applications. Indeed, various approaches to control wettability using FS laser-fabricated surface micro/nanostructure have been explored recently. As a result, superwetting responses, including superhydrophobic–superoleophilic, superhydrophilic–underwater superoleophobic, underwater superoleophobic, and underoil superhydrophobic responses, have been demonstrated for such surfaces and have shown promising results with respect to oil–water separation. This approach has some advantages compared with competitive oil–water separation techniques as far as the durability of the fabricated oil–water separation systems. Specifically, alternative technologies usually employ fragile and low-adhesion fluorinated compounds that lose their superwetting characteristic over a short period of time. On the contrary, FS laser-induced surface structuring can provide surface structures in a single step, without the need for additional chemical coatings. As a result, FS laser-structured filters/membranes have shown promising results of high efficiency, recyclability, and durability with respect to oil–water separation. Oil–water separation by FS laser surface structuring has been realized in two ways, namely meshes decorated with self-organized structures and arrays of microholes created by laser ablation. In both cases, surface structuring may also be followed by a chemical functionalization step. Both meshes and micro-through holes filters have been used for the separation of heavy and light oil/water mixtures.

Although, FS laser surface structures display exceptional oil–water separation efficiency on a laboratory scale, their potential use for separating large volumes of oil–water mixtures in oil spill accidents and organic wastes in industries requires further research. It should be considered that in

most of the separation studies, self-prepared oil–water mixtures have been used, which do not perfectly simulate the properties of real oil–water mixtures present in oil leakages and spills. Indeed, oil spills and organic industrial wastes consist of an amalgam of hydrocarbons of different densities, including thick crude oil, emulsions, and surfactants, which could cause fouling and blockage of the micropores present in separation systems. In this context, studies addressing the separation of emulsions and impure organic compounds via FS laser-structured separation systems should be performed. Another study that requires special attention is that of separation at high flux rates, mostly related to the systems used for continuous separation of oil–water mixtures.

Finally, it should be emphasized that the use of FS laser-generated self-organized surface structures for oil–water separation is still considerably limited. To date, only LISR have been used; however, this is not the case for membranes decorated with LISG and LISS structures. Moreover, the use of FS high-pulse energies in laser micromachining via ablation has not been explored yet. The surface structures formed as a result of high-pulse energy laser ablation are expected to provide exceptional results. These studies will also be useful in adapting this technology to large-area membrane systems fabricated in a short period of time.

Considering that oil–water separation via FS laser surface structuring is still in its infancy, significant development is expected on this topic in the near future. This is further supported by the few preliminary but encouraging results on the application of FS laser surface structuring for oil–water separation purposes. It is thus envisaged that FS laser surface structuring will become a unique tool in high-end oil-water separation applications.

Author Contributions: Conceptualization, A.S.A.; Investigation, S.A.K.; Writing-Original Draft Preparation, S.A.K and A.S.A.; Writing-Review and Editing, S.A.K, A.S.A., R.A.G, E.S., Supervision, A.S.A.

Funding: This research was supported by the office of research at the American University of Sharjah.

Acknowledgments: A.S.A. and S.A.K. acknowledge support from the American University of Sharjah.

Conflicts of Interest: The authors declare no conflicts of interest.

References

1. Miyaji, G.; Miyazaki, K. Origin of periodicity in nanostructuring on thin film surfaces ablated with femtosecond laser pulses. *Opt. Express* **2008**, *16*, 16265. [CrossRef]
2. Stratakis, E. Nanomaterials by ultrafast laser processing of surfaces. *Sci. Adv. Mater.* **2012**, *4*, 407–431. [CrossRef]
3. Vorobyev, A.Y.; Guo, C. Direct femtosecond laser surface nano/microstructuring and its applications. *Laser Photonics Rev.* **2013**, *7*, 385–407. [CrossRef]
4. Vorobyev, A.Y.; Guo, C. Femtosecond laser blackening of platinum. *J. Appl. Phys.* **2008**, *104*, 053516. [CrossRef]
5. Kontermann, S.; Gimpel, T.; Baumann, A.L.; Guenther, K.-M.; Schade, W. Laser Processed Black Silicon for Photovoltaic Applications. *Energy Procedia* **2012**, *27*, 390–395. [CrossRef]
6. Sygletou, M.; Petridis, C.; Kymakis, E.; Stratakis, E. Advanced Photonic Processes for Photovoltaic and Energy Storage Systems. *Adv. Mater.* **2017**, *29*, 1700335. [CrossRef]
7. Zhao, L.; Feng, G.; Xiao, S.; Zhu, B.; Zhou, L.; Li, Y.; Zhang, S. Strong infrared absorber: Surface-microstructured Au film replicated from black silicon. *Opt. Express* **2011**, *19*, 20462.
8. Vorobyev, A.Y.; Guo, C. Metal colorization with femtosecond laser pulses. In *High-Power Laser Ablation VII*; Phipps, C.R., Ed.; International Society for Optics and Photonics: Bellingham, WA, USA, 2008; Volume 7005, p. 70051T.
9. Vorobyev, A.Y.; Guo, C. Colorizing metals with femtosecond laser pulses. *Appl. Phys. Lett.* **2008**, *92*, 1–4. [CrossRef]
10. Yao, J.; Zhang, C.; Liu, H.; Dai, Q.; Wu, L.; Lan, S.; Gopal, A.V.; Trofimov, V.A.; Lysak, T.M. Selective appearance of several laser-induced periodic surface structure patterns on a metal surface using structural colors produced by femtosecond laser pulses. *Appl. Surf. Sci.* **2012**, *258*, 7625–7632. [CrossRef]

11. Long, J.; Fan, P.; Gong, D.; Jiang, D.; Zhang, H.; Li, L.; Zhong, M. Superhydrophobic Surfaces Fabricated by Femtosecond Laser with Tunable Water Adhesion: From Lotus Leaf to Rose Petal. *ACS Appl. Mater. Interfaces* **2015**, *7*, 9858–9865. [CrossRef] [PubMed]
12. Stratakis, E.; Ranella, A.; Fotakis, C. Biomimetic micro/nanostructured functional surfaces for microfluidic and tissue engineering applications. *Biomicrofluidics* **2011**, *5*, 013411. [CrossRef] [PubMed]
13. Lu, J.; Ngo, C.-V.; Singh, S.C.; Yang, J.; Xin, W.; Yu, Z.; Guo, C. Bioinspired Hierarchical Surfaces Fabricated by Femtosecond Laser and Hydrothermal Method for Water Harvesting. *Langmuir* **2019**, *35*, 3562–3567. [CrossRef] [PubMed]
14. Vorobyev, A.Y.; Guo, C. Metal pumps liquid uphill. *Appl. Phys. Lett.* **2009**, *94*, 2007–2010. [CrossRef]
15. Paradisanos, I.; Fotakis, C.; Anastasiadis, S.H.; Stratakis, E. Gradient induced liquid motion on laser structured black Si surfaces. *Appl. Phys. Lett.* **2015**, *107*, 111603. [CrossRef]
16. Yang, L.; Chen, T.; Yang, Q.; Wu, W.J.; Fan, S.; Duan, X.M. Controllable wettability of metallic surfaces via micro-nano structure fabricated by femtosecond laser. In Proceedings of the 9th International Symposium on Advanced Optical Manufacturing and Testing Technologies: Subdiffraction-Limited Plasmonic Lithography and Innovative Manufacturing Technology 2019, Chengdu, China, 26–29 June 2019; Volume 10842.
17. Allahyari, E.; Ausanio, G.; Vecchione, A.; Amoruso, S.; Oscurato, S.L.; Salvatore, M.; Fittipaldi, R.; Bruzzese, R.; Nivas, J.; Maddalena, P. Laser surface texturing of copper and variation of the wetting response with the laser pulse fluence. *Appl. Surf. Sci.* **2018**, *470*, 817–824. [CrossRef]
18. Chen, G.; Wang, Z.K.; Zheng, H.Y.; Thwe, A.M.; Lam, Y.C. Investigation on polycarbonate surface wetting property with femtosecond laser irradiation and ultrasonic treatment. *Opt. Laser Technol.* **2019**, *115*, 316–324. [CrossRef]
19. Huerta-Murillo, D.; García-Girón, A.; Romano, J.M.; Cardoso, J.T.; Cordovilla, F.; Walker, M.; Dimov, S.S.; Ocaña, J.L. Wettability modification of laser-fabricated hierarchical surface structures in Ti-6Al-4V titanium alloy. *Appl. Surf. Sci.* **2019**, *463*, 838–846. [CrossRef]
20. Xi, M.; Yong, J.; Chen, F.; Yang, Q.; Hou, X. A femtosecond laser-induced superhygrophobic surface: Beyond superhydrophobicity and repelling various complex liquids. *RSC Adv.* **2019**, *9*, 6650–6657. [CrossRef]
21. Vorobyev, A.Y.; Guo, C. Femtosecond laser structuring of titanium implants. *Appl. Surf. Sci.* **2007**, *253*, 7272–7280. [CrossRef]
22. Ranella, A.; Barberoglou, M.; Bakogianni, S.; Fotakis, C.; Stratakis, E. Tuning cell adhesion by controlling the roughness and wettability of 3D micro/nano silicon structures. *Acta Biomater.* **2010**, *6*, 2711–2720. [CrossRef]
23. Charalampopoulos, I.; Kourgiantaki, A.; Athanassakis, I.; Efstathopoulos, P.; Fotakis, C.; Ranella, A.; Stratakis, E.; Gravanis, A.; Simitzi, C. Laser fabricated discontinuous anisotropic microconical substrates as a new model scaffold to control the directionality of neuronal network outgrowth. *Biomaterials* **2015**, *67*, 115–128.
24. Buividas, R.; Stoddart, P.R.; Juodkazis, S. Laser fabricated ripple substrates for surface-enhanced Raman scattering. *Ann. Phys.* **2012**, *524*, 1–6. [CrossRef]
25. Bonse, J.; Koter, R.; Hartelt, M.; Spaltmann, D.; Pentzien, S.; Höhm, S.; Rosenfeld, A.; Krüger, J. Tribological performance of femtosecond laser-induced periodic surface structures on titanium and a high toughness bearing steel. *Appl. Surf. Sci.* **2015**, *336*, 21–27. [CrossRef]
26. Putignano, C.; Scarati, D.; Gaudiuso, C.; Di Mundo, R.; Ancona, A.; Carbone, G. Soft matter laser micro-texturing for friction reduction: An experimental investigation. *Tribol. Int.* **2019**, *136*, 82–86. [CrossRef]
27. Vorobyev, A.Y.; Guo, C. Femtosecond laser nanostructuring of metals. *Opt. Express* **2006**, *14*, 2164. [CrossRef] [PubMed]
28. Jia, T.; Baba, M.; Suzuki, M.; Ganeev, R.A.; Kuroda, H.; Qiu, J.; Wang, X.; Li, R.; Xu, Z.; Liang, G.; et al. Fabrication of two-dimensional periodic nanostructures by two-beam interference of femtosecond pulses. *Nanoeng. Adv. Polym. Sci* **2005**, *72*, 125429–125433. [CrossRef]
29. Chen, F.; Zhang, D.; Yang, Q.; Yong, J.; Du, G.; Si, J.; Yun, F.; Hou, X. Bioinspired wetting surface via laser microfabrication. *ACS Appl. Mater. Interfaces* **2013**, *5*, 6777–6792. [CrossRef]
30. Skoulas, E.; Manousaki, A.; Fotakis, C.; Stratakis, E. Biomimetic surface structuring using cylindrical vector femtosecond laser beams. *Sci. Rep.* **2017**, *7*, 45114. [CrossRef]

31. Martínez-Calderon, M.; Rodríguez, A.; Dias, A.; Gómez-Aranzadi, M.; Olazoila, S.M. Femtosecond laser manufacturing of highly hydrophobic hierarchical structures fabricated by combining surface microstructures and LIPSS. In Proceedings of the Lasers in Manufacturing Conference, Munich, Germany, 15–22 June 2015.
32. Yong, J.; Chen, F.; Yang, Q.; Jiang, Z.; Hou, X. A Review of Femtosecond-Laser-Induced Underwater Superoleophobic Surfaces. *Adv. Mater. Interfaces* **2018**, *5*, 1870033. [CrossRef]
33. Giannuzzi, G.; Gaudiuso, C.; Cinquino, M.; Di Mundo, R.; Mirenghi, L.; Di Franco, C.; Scamarcio, G.; Lugarà, P.M.; Ancona, A. 1-D and 2-D surface structuring of steel by bursts of femtosecond laser pulses. In Proceedings of the Laser-Based Micro-and Nanoprocessing XIII, San Francisco, CA, USA, 2–7 February 2019; Volume 10906.
34. Tanvir Ahmmed, K.M.; Grambow, C.; Kietzig, A.M. Fabrication of micro/nano structures on metals by femtosecond laser micromachining. *Micromachines* **2014**, *5*, 1219–1253. [CrossRef]
35. Tsibidis, G.D.; Fotakis, C.; Stratakis, E. From ripples to spikes: A hydrodynamical mechanism to interpret femtosecond laser-induced self-assembled structures. *Phys. Rev. B Condens. Matter Mater. Phys.* **2015**, *92*, 1–6. [CrossRef]
36. Bonse, J.; Höhm, S.; Kirner, S.; Rosenfeld, A.; Krüger, J. Laser-induced Periodic Surface Structures (LIPSS)—A Scientific Evergreen. In *CLEO: Science and Innovations*; Optical Society of America: Tucson, AZ, USA, 2016.
37. Birnbaum, M. Semiconductor surface damage produced by Ruby lasers. *J. Appl. Phys.* **1965**, *36*, 3688–3689. [CrossRef]
38. Li, G.; Li, J.; Hu, Y.; Zhang, C.; Li, X.; Chu, J.; Huang, W. Femtosecond laser color marking stainless steel surface with different wavelengths. *Appl. Phys. A Mater. Sci. Process.* **2014**, *118*, 1189–1196. [CrossRef]
39. Yong, J.; Chen, F.; Yang, Q.; Hou, X. Femtosecond laser controlled wettability of solid surfaces. *Soft Matter* **2015**, *11*, 8897–8906. [CrossRef]
40. Gräf, S.; Müller, F.A. Polarisation-dependent generation of fs-laser induced periodic surface structures. *Appl. Surf. Sci.* **2015**, *331*, 150–155. [CrossRef]
41. Tsibidis, G.D.; Skoulas, E.; Stratakis, E. Ripple formation on nickel irradiated with radially polarized femtosecond beams. *Opt. Lett.* **2015**, *40*, 5172. [CrossRef]
42. Hermens, U.; Kirner, S.V.; Emonts, C.; Comanns, P.; Skoulas, E.; Mimidis, A.; Mescheder, H.; Winands, K.; Krüger, J.; Stratakis, E.; et al. Mimicking lizard-like surface structures upon ultrashort laser pulse irradiation of inorganic materials. *Appl. Surf. Sci.* **2017**, *418*, 499–507. [CrossRef]
43. Stratakis, E.; Zorba, V.; Barberoglou, M.; Fotakis, C.; Shafeev, G.A. Laser writing of nanostructures on bulk Al via its ablation in liquids. *Nanotechnology* **2009**, *20*, 105303. [CrossRef]
44. Nayak, B.K.; Gupta, M.C. Self-organized micro/nano structures in metal surfaces by ultrafast laser irradiation. *Opt. Lasers Eng.* **2010**, *48*, 940–949. [CrossRef]
45. Nayak, B.K.; Gupta, M.C.; Kolasinski, K.W. Formation of nano-textured conical microstructures in titanium metal surface by femtosecond laser irradiation. *Appl. Phys. A Mater. Sci. Process.* **2008**, *90*, 399–402. [CrossRef]
46. Yong, J.; Chen, F.; Yang, Q.; Zhang, D.; Farooq, U.; Du, G.; Hou, X. Bioinspired underwater superoleophobic surface with ultralow oil-adhesion achieved by femtosecond laser microfabrication. *J. Mater. Chem. A* **2014**, *2*, 8790–8795. [CrossRef]
47. Zorba, V.; Stratakis, E.; Barberoglou, M.; Spanakis, E.; Tzanetakis, P.; Anastasiadis, S.H.; Fotakis, C. Biomimetic artificial surfaces quantitatively reproduce the water repellency of a lotus leaf. *Adv. Mater.* **2008**, *20*, 4049–4054. [CrossRef]
48. Subhash Latthe, S.; Basavraj Gurav, A.; Shridhar Maruti, C.; Shrikant Vhatkar, R. Recent Progress in Preparation of Superhydrophobic Surfaces: A Review. *J. Surf. Eng. Mater. Adv. Technol.* **2012**, *2*, 76–94. [CrossRef]
49. Lin, Y.; Chen, H.; Wang, G.; Liu, A. Recent Progress in Preparation and Anti-Icing Applications of Superhydrophobic Coatings. *Coatings* **2018**, *8*, 208. [CrossRef]
50. Wang, H.; Hu, X.; Ke, Z.; Du, C.Z.; Zheng, L.; Wang, C.; Yuan, Z. Review: Porous Metal Filters and Membranes for Oil–Water Separation. *Nanoscale Res. Lett.* **2018**, *13*, 284. [CrossRef]
51. Wenzel, R.N. Resistance of solid surfaces to wetting by water. *Ind. Eng. Chem.* **1936**, *28*, 988–994. [CrossRef]
52. Cassie, A.B.D.; Baxter, S. Wettability of porous surfaces. *Trans. Faraday Soc.* **1944**, *40*, 546–551. [CrossRef]
53. Marmur, A. Wetting on hydrophobic rough surfaces: To be heterogeneous or not to be? *Langmuir* **2003**, *19*, 8343. [CrossRef]
54. Feng, L.; Zhang, Z.; Mai, Z.; Ma, Y.; Liu, B.; Jiang, L.; Zhu, D. A super-hydrophobic and super-oleophilic coating mesh film for the separation of oil and water. *Angew. Chem. Int. Ed.* **2004**, *43*, 2012–2014. [CrossRef]

55. Khan, S.A.; Zulfiqar, U.; Hussain, S.Z.; Zaheer, U.; Hussain, I.; Husain, S.W.; Subhani, T. Fabrication of superhydrophobic filter paper and foam for oil–water separation based on silica nanoparticles from sodium silicate. *J. Sol-Gel Sci. Technol.* **2017**, *81*, 912–920. [CrossRef]
56. Zulfiqar, U.; Hussain, S.Z.; Awais, M.; Khan, M.M.J.; Hussain, I.; Husain, S.W.; Subhani, T. In-situ synthesis of bi-modal hydrophobic silica nanoparticles for oil-water separation. *Colloids Surf. A Physicochem. Eng. Asp.* **2016**, *508*, 301–308. [CrossRef]
57. Liu, F.; Ma, M.; Zang, D.; Gao, Z.; Wang, C. Fabrication of superhydrophobic/superoleophilic cotton for application in the field of water/oil separation. *Carbohydr. Polym.* **2014**, *103*, 480–487. [CrossRef]
58. Lei, S.; Shi, Z.; Ou, J.; Wang, F.; Xue, M.; Li, W.; Qiao, G.; Guan, X.; Zhang, J. Durable superhydrophobic cotton fabric for oil/water separation. *Colloids Surf. A Physicochem. Eng. Asp.* **2017**, *533*, 249–254. [CrossRef]
59. Yong, J.; Chen, F.; Huo, J.; Fang, Y.; Yang, Q.; Bian, H.; Li, W.; Wei, Y.; Dai, Y.; Hou, X. Green, Biodegradable, Underwater Superoleophobic Wood Sheet for Efficient Oil/Water Separation. *ACS Omega* **2018**, *3*, 1395–1402. [CrossRef]
60. Li, J.; Yan, L.; Hu, W.; Li, D.; Zha, F.; Lei, Z. Facile fabrication of underwater superoleophobic TiO_2 coated mesh for highly efficient oil/water separation. *Colloids Surf. A Physicochem. Eng. Asp.* **2016**, *489*, 441–446. [CrossRef]
61. Wu, L.; Li, L.; Li, B.; Zhang, J.; Wang, A. Magnetic, durable, and superhydrophobic polyurethane@Fe_3O_4@SiO_2@fluoropolymer sponges for selective oil absorption and oil/water separation. *ACS Appl. Mater. Interfaces* **2015**, *7*, 4936–4946. [CrossRef]
62. Gupta, R.K.; Dunderdale, G.J.; England, M.W.; Hozumi, A. Oil/water separation techniques: A review of recent progresses and future directions. *J. Mater. Chem. A* **2017**, *5*, 16025–16058. [CrossRef]
63. Ge, M.; Cao, C.; Huang, J.; Zhang, X.; Tang, Y.; Zhou, X.; Zhang, K.; Chen, Z.; Lai, Y. Rational design of materials interface at nanoscale towards intelligent oil-water separation. *Nanoscale Horiz.* **2018**, *3*, 235–260. [CrossRef]
64. Xue, Z.; Wang, S.; Lin, L.; Chen, L.; Liu, M.; Feng, L.; Jiang, L. A novel superhydrophilic and underwater superoleophobic hydrogel-coated mesh for oil/water separation. *Adv. Mater.* **2011**, *23*, 4270–4273. [CrossRef]
65. Hou, Y.; Wang, Z.; Guo, J.; Shen, H.; Zhang, H.; Zhao, N.; Zhao, Y.; Chen, L.; Liang, S.; Jin, Y.; et al. Facile fabrication of robust superhydrophobic porous materials and their application in oil/water separation. *J. Mater. Chem. A* **2015**, *3*, 23252–23260. [CrossRef]
66. Liu, Y.-Q.; Han, D.-D.; Jiao, Z.-Z.; Liu, Y.; Jiang, H.-B.; Wu, X.-H.; Ding, H.; Zhang, Y.-L.; Sun, H.-B. Laser-structured Janus wire mesh for efficient oil–water separation. *Nanoscale* **2017**, *9*, 17933–17938. [CrossRef]
67. Yin, K.; Chu, D.; Dong, X.; Wang, C.; Duan, J.-A.; He, J. Femtosecond laser induced robust periodic nanoripple structured mesh for highly efficient oil–water separation. *Nanoscale* **2017**, *9*, 14229–14235. [CrossRef]
68. Yong, J.; Fang, Y.; Chen, F.; Huo, J.; Yang, Q.; Bian, H.; Du, G.; Hou, X. Femtosecond laser ablated durable superhydrophobic PTFE films with micro-through-holes for oil/water separation: Separating oil from water and corrosive solutions. *Appl. Surf. Sci.* **2016**, *389*, 1148–1155. [CrossRef]
69. Ye, S.; Cao, Q.; Wang, Q.; Wang, T.; Peng, Q. A highly efficient, stable, durable, and recyclable filter fabricated by femtosecond laser drilling of a titanium foil for oil-water separation. *Sci. Rep.* **2016**, *6*, 1–9. [CrossRef]
70. Li, G.; Fan, H.; Ren, F.; Zhou, C.; Zhang, Z.; Xu, B.; Wu, S.; Hu, Y.; Zhu, W.; Li, J.; et al. Multifunctional ultrathin aluminum foil: Oil/water separation and particle filtration. *J. Mater. Chem. A* **2016**, *4*, 18832–18840. [CrossRef]
71. Kietzig, A.M.; Hatzikiriakos, S.G.; Englezos, P. Patterned superhydrophobic metallic surfaces. *Langmuir* **2009**, *25*, 4821–4827. [CrossRef]
72. Yong, J.; Singh, S.C.; Zhan, Z.; Chen, F.; Guo, C. How To Obtain Six Different Superwettabilities on a Same Microstructured Pattern: Relationship between Various Superwettabilities in Different Solid/Liquid/Gas Systems. *Langmuir* **2019**, *35*, 921–927. [CrossRef]
73. Yong, J.; Chen, F.; Li, M.; Yang, Q.; Fang, Y.; Huo, J.; Hou, X. Remarkably simple achievement of superhydrophobicity, superhydrophilicity, underwater superoleophobicity, underwater superoleophilicity, underwater superaerophobicity, and underwater superaerophilicity on femtosecond laser ablated PDMS surfaces. *J. Mater. Chem. A* **2017**, *5*, 25249–25257. [CrossRef]